

Contents lists available at ScienceDirect

Petroleum Science

journal homepage: www.keaipublishing.com/en/journals/petroleum-science



Original Paper

Adsorption and retention of fracturing fluid and its impact on gas transport in tight sandstone with different clay minerals



Yi-Jun Wang ^a, Li-Jun You ^a, Jian Yang ^b, Yi-Li Kang ^a, Ming-Jun Chen ^a, Jia-Jia Bai ^{a, d}, Jian Tian ^{c, *}

- ^a State Key Laboratory of Oil and Gas Reservoir Geology and Exploitation, Southwest Petroleum University, Chengdu, 610500, Sichuan, China
- ^b Engineering Technology Research Institute of Southwest Oil & Gas Field Company, PetroChina, Chengdu, 610017, Sichuan, China
- ^c State Key Laboratory of Coal Mine Disaster Dynamics and Control, Chongqing University, Chongqing, 400044, China
- ^d School of Petroleum Engineering, Changzhou University, Changzhou, 213164, Jiangsu, China

ARTICLE INFO

Article history: Received 19 March 2024 Received in revised form 12 September 2024 Accepted 13 September 2024 Available online 14 September 2024

Edited by Yan-Hua Sun

Keywords: Clay minerals Formation damage Fracturing fluid retention distribution Adsorption morphology

ABSTRACT

To elucidate the adsorption characteristics and retention mechanisms of fracturing fluids in diverse clay minerals, we conducted on-line nuclear magnetic resonance (NMR) and atomic force microscopy (AFM) experiments. The depth and extent of solid phase damage are determined by the ratio between the size of fine fractions in fracturing fluid residue and the pore-throat size in experiments. Poor physical properties (K < 0.5 mD) result in a more preferential flow pathway effect during flowback, and the stepwise incremental pressure differential proves to be more effective for the discharge of fracturing fluid in submicron pore throats. The permeability is significantly influenced by the differential distribution of retained fracturing fluid, as supported by direct experimental evidence. The presence of good physical properties (K > 0.5 mD) combined with a scattered distribution of retained fracturing fluid is associated with high gas phase recovery permeability, whereas a continuous sheet-like distribution results in low recovery permeability. The expansive surface area and presence of filamentous illite minerals facilitate the multiple winding and adsorption of fracturing fluids, demonstrating strong hydrogen-bonding, multi-layering and multiple adsorption properties. The geological characteristics of the main gas formations exhibit significant variation, and the severity of damage caused by fracturing fluids occurs in diverse sequences. To address this issue, a differentiated strategy for optimizing fracturing fluids has been proposed.

© 2024 The Authors. Publishing services by Elsevier B.V. on behalf of KeAi Communications Co. Ltd. This is an open access article under the CC BY-NC-ND license (http://creativecommons.org/licenses/by-nc-nd/

4.0/).

1. Introduction

The escalating energy demand and implementation of the carbon capture utilization and storage (CCUS) policy have influenced the surge in exploration and development of natural gas, specifically for tight sandstone gas, which is now a significant area of contemporary research (Anderson and Rezaie, 2019; Xin et al., 2021). In China, tight sandstone gas is plentifully dispersed in the Ordos, Sichuan, Tarim, Songliao, Bohai Bay, and other Chinese basins (Sun et al., 2019; Lai et al., 2019), with an estimated resource of approximately 21.85 \times 10¹² m³. In terms of technological maturity and industrialization scale, it is the most important unconventional

* Corresponding author.

E-mail address: tianjian2171@cqu.edu.cn (J. Tian).

natural gas resource in China with the most realistic significance for exploration and development (Kang and Luo, 2007; Wang et al., 2021). However, tight gas development is currently facing many challenges such as declining resource quality and severe heterogeneity, and most reservoirs must rely on hydraulic fracturing to achieve industrial production (Tian et al., 2020; Wu et al., 2017; Cai et al., 2020). During hydraulic fracturing operations, fracturing fluids are used to transfer pressure, carry sand to induce fractures, and deliver proppant into the fractures, which is fundamental to the success of hydraulic fracturing (Zhang Y. et al., 2019; Guo and He, 2012). Nevertheless, it unavoidably triggers formation damage and impedes the enhancement of permeability to a certain degree. It is well known that formation damage is a process that impedes gas mass transfer and affects gas transport capacity (Wang et al., 2021). In certain severe cases, fracturing fluids became significantly trapped within the formation and displayed

incompatibility with the rock, leading to a notable decrease in production or the creation of unproductive gas wells (Xu et al., 2016; Guo et al., 2018b). Therefore, it is crucial to precisely comprehend the adsorption and retention of fracturing fluids for the effective advancement of oil and gas reserves.

The type of formation damage resulting from fracturing fluids is primarily determined by the specific composition of the fracturing fluid, as well as the mineral composition and pore structure of the formation (Guo et al., 2018a). Over 90% of fracturing fluid varieties are water-based, and unconventional reservoirs are primarily fractured using hydroxypropyl guar (HPG) and slick water (Chitrala et al., 2013). The natural polysaccharide hydroxypropyl guar is added to the fracturing fluid as a thickener to improve its ability to carry proppant (Guo et al., 2018a). However, high viscosity will reduce its flowback efficiency and cause formation damage (Tian et al., 2020). The residue and polymer formed by incomplete degradation of HPG fracturing fluid after breaking gel will be retained in the fracture, which restricts the flow conductivity to a certain extent (Li et al., 2022). For the matrix adjacent to the fracture surface, residues of the fine fraction of the fracturing fluid and some polymer insolubles can enter the pore space and cause solid phase damage to the matrix (Kang et al., 2014). When the fracturing pump is stopped, the fracturing fluid filtrate will infiltrate the matrix pores due to forced imbibition (Xu et al., 2020; Cai et al., 2021). This can trap most of the liquid in small pores and cause the water phase to occupy the gas phase seepage pathway, manifested as strong water phase trapping (WPT) damage (Wang et al., 2022). During the production process, as the pore pressure drops, part of retained fracturing fluid filtrate is produced with the gas phase, leading to early water production and significant loss of productivity (Tian et al., 2022). A meticulous analysis of the spatial and temporal distribution of the retained fracturing fluids in the pore space is crucial to enhance the efficiency of fracturing fluid drainage and the gas production capacity of gas formations. The investigation of the evolution of gas-water distribution and the response of flow mechanisms presents a myriad of potential applications in the development of oil and gas resources and the utilization of underground spaces (Xu et al., 2020). However, the majority of present research on the invasion and drainage of fracturing fluid is founded on static displacement experiments conducted at the core-scale (Song et al., 2018; Liang et al., 2017). These experiments are similar to black-box experiments and cannot illustrate the mechanism responsible for the retention of fracturing fluids in the pore space or the capillary trapping events (Guo et al., 2018a; Li et al., 2022).

In addition to the damage caused by the solid and liquid phases of fracturing fluid, the adsorption retention damage inflicted by HPG fracturing fluid on rock pore throat surfaces poses a significant impediment to the widespread adoption of water-based fracturing fluids (Fu et al., 2020; Li et al., 2019). The molecules of the thickener, predominantly hydroxypropyl guar gum, adhere to and remain in the porous medium of the rock (Fu et al., 2020). The adsorption of HPG polymer on the rock surface is predominantly analyzed through direct and indirect methods. The direct method primarily involves the decomposition of heating to determine mass changes, which reflects the degree of adsorption. Indirect methods, such as ultraviolet (UV) spectroscopy and total carbon analysis, determine the quantity of thickening additive molecules adsorbed in the fracturing liquid by examining the change in concentration before and after contact with the rock (Guo et al., 2018a; Li et al., 2019). The relationship between the amount of fracturing fluid adsorbed and the degree of damage is often not a simple linear relationship but has some correlation with the adsorption morphology of fracturing fluids. The morphology of HPG fracturing fluid's adsorption and retention in rock can be analyzed using scanning electron

microscope (SEM), transmission electron microscope (TEM), atomic force microscopy (AFM), and molecular simulation techniques (Zhang et al., 2018; Pennycook et al., 1988; Eysden et al., 2008). However, the mineral composition and pore structure of formations, particularly the type and content of clay minerals, have a significant influence on fracturing fluid's adsorption and retention in rocks (Guo et al., 2018a). Currently, there is a relative lack of research regarding the adsorption and damage of various physical properties, lithologies, and clay mineral microstructures in relation to fracturing fluid adsorption. Additionally, to the best of our knowledge, no study has systematically revealed the correlation mechanism between the microstructure of clay minerals and the adsorption and retention of fracturing fluids.

To gain a deeper understanding of the comprehensive damage characteristics of fracturing fluids in three types of clay mineral tight sandstone gas reservoirs, we conducted multiple experiments. Firstly, high-temperature and high-pressure (HTHP) dynamic evaluation experimentals and on-line NMR measurements were performed under formation condition to analyze the mechanisms of the fracturing fluid damage. Subsequently, SEM and AFM observations were employed to study the fracturing fluid adsorption morphology and damage characteristics. Finally, a differentiated strategy for optimizing fracturing fluids was proposed.

2. Methodology

2.1. Sample description

2.1.1. Rock samples

The adsorption and retention behavior of fracturing fluid in tight sandstones is significantly influenced by the presence of clay minerals. Consequently, this study has chosen gas reservoirs in tight sandstones that are enriched with three distinct types of clay minerals. The study block lies on the eastern margin of the Ordos Basin, which borders the tectonic edge of the basin (Lai et al., 2019; Zhang et al., 2020). The gas-bearing layers from top to bottom include the Upper Shihezi Formation (USF), Lower Shihezi Formation (LSF), and Taiyuan Formation (TF). The primary clay minerals present are chlorite, kaolinite, and illite, respectively (Fig. 1) (Zhang et al., 2020). Considering the gas formation in the study block occurs within a closed environment characterized by high mineralization of formation water, the experimental cores underwent saltwashing using alcohol and organic solvents prior to all testing. Basic physical properties of the samples tested are listed in Table 1. The samples from different layers exhibit a porosity range of 6.90%-13.36% and a permeability range of 0.15-1.33 mD.

2.1.2. Experimental fluids

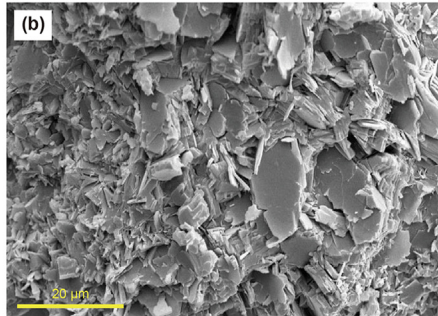
The experimental fluids mainly include simulated formation water and HPG fracturing fluid. The configuration of simulated formation water is mainly based on the results of sealed coring in the field. The composition of the fracturing fluid comprises 0.3% guar gum, 0.1% fungicide, 0.5% clay stabilizer, 0.3% cleanup additive, 0.1% pH regulator, 0.15% crosslinking additive, 0.03% gel breaker, and 10 ppm biological enzyme. The viscosity and residue content after gel breaking are 2.85 mPa·s and 350.45 mg/L, respectively. According to the standard SY/T 5107-2016, the HPG fracturing fluid filtrate was prepared in the laboratory.

2.2. Experimental methods

2.2.1. Dynamic and static damage evaluation of fracturing fluid

The dynamic damage ratio, which reflects the comprehensive damage caused by fracturing fluid, holds significant importance as one of the key parameters for optimizing fracturing fluid in





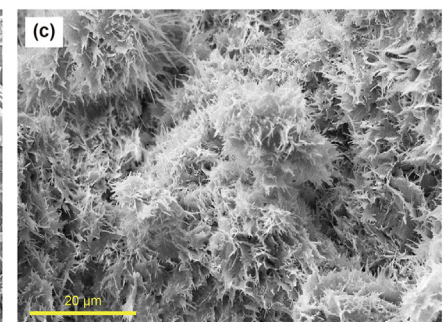


Fig. 1. Typical SEM photos of different gas layers: (a) USF, mainly composed of chlorite; (b) LSF, mainly composed of kaolinite; (c) TF, mainly composed of filamentous illite.

Table 1Basic parameters of the selected rock samples.

Sample	Depth, m	Length, cm	Diameter, cm	Porosity, %	Permeability, mD	Gas layer type
U-1	1690.97	4.07	2.53	13.36	1.33	USF
U-2	1693.85	5.30	2.53	11.90	0.86	
L-1	1732.75	5.80	2.55	10.50	0.30	LSF
L-2	1838.74	5.90	2.60	7.10	0.15	
T-1	1900.36	5.11	2.41	9.90	0.38	TF
T-2	1904.04	4.99	2.52	6.90	0.16	

hydraulic fracturing operations. The experiment employed a self-made HTHP instrument for evaluating dynamic damage caused by working fluid. A detailed introduction of the device can be found in our earlier work (Wang et al., 2021; Kang et al., 2014). The specific steps include (Kang et al., 2014): (1) Determine the initial formation conditions, including setting the initial water saturation, temperature and effective stress. (2) The initial benchmark permeability was tested and a 1 MPa back pressure was applied at the outlet to eliminate the gas slippage effect. (3) The fracturing fluid was injected into the core for dynamic cyclic shear at a constant pressure of 3.5 MPa. (4) Variable pressure differential gas flooding experiment was carried out. (5) SEM observation was carried out on the leading, central, and rear regions of the core.

The experimental fluid employed to evaluate the static damage evaluation of fracturing fluid is filtrate from gel breaking, and the specific experimental steps are detailed below (Zhang D.J. et al., 2019): (1) Filter and prepare the gel breaking fluid filtrate. (2) Put the core into the holder, establish the initial water saturation, and measure the baseline permeability. (3) Inject the fracturing fluid filtrate into the core under the condition of constant pressure of 3.5 MPa to simulate the process of forced seepage and intrusion into the matrix at a certain pressure after stopping the pump. (4) Conduct constant pressure differential and increasing pressure differential test.

2.2.2. WPT damage evaluation with on-line NMR measurement

The challenge of consistently obtaining measurements of water saturation changes using a core displacement experiment can be resolved through the implementation of an online NMR device. The NMR relaxation signal can accurately reflect the hydrogen nucleus (¹H) signal within the pores, subsequently indicating petrophysical properties and fluid flow characteristics indirectly (Yang et al., 2023; Bai et al., 2019; Yao et al., 2010). The HTHP core displacement experimental apparatus equipped with the on-line NMR multi-sequence test function is exhibited in Fig. 2. The experimental facility comprises an injection system, an NMR testing system, and a metrological analysis system, with a temperature resistance of 120 °C and a pressure resistance of 40 MPa.

The Carr-Purcell-Meiboom-Gill (CPMG) sequence was mainly

used to measure the T_2 spectral curves, and the spin-echo single point imaging (SE-SPI) sequence was used to measure the layered visualization maps along the radial direction of the core. The waiting time, echo interval time, number of echoes, and number of scans were set to 5000 ms, 0.5 ms, 18000, and 64, respectively, in the low-field NMR experiments. The procedures for unsteady-state gas displacement with on-line NMR measurements are briefly described as follows (Wang et al., 2021; Tian et al., 2020): (1) Prior to each experiment, the core samples were vacuumed and fully saturated with configured simulated formation water for 48 h (2) The center frequency calibration and uniform field parameter tuning of the low field NMR instrument were carried out. (3) Cores saturated with formation water were placed in a holder to simulate reservoir conditions, and 17 MPa of confining pressure and 1 MPa of back pressure were applied to the cores, respectively (Tian et al., 2020). (4) Test the NMR T_2 spectral curves of water-saturated cores, and use it as the benchmark value of NMR spectra. (5) Two types of experiments were carried out: constant pressure gas displacement and gradually increasing pressure differential gas displacement, and the NMR T2 spectral curves and SE-SPI visualization maps were tested every 20 min.

2.2.3. Evaluation of HPG fracturing fluid adsorption damage

Anthrone colorimetry was employed to assess the static and dynamic adsorption of fracturing fluids on various clay minerals of tight sandstones (Guo et al., 2018a). The static adsorption steps are as follows: (1) Prepare the ethyl acetate-anthracenone solution and carry out a reaction using a water bath at 90 °C for 10 min. After cooling for 10 min, measure the absorbance using a UV spectrometer. (2) Vary the concentration of HPG fracturing solution and repeat the previous steps. Then, use curve-fitting techniques to obtain the concentration of HPG fracturing solution and the UV absorbance of the standard curve. (3) Determination of the saturated static adsorption of HPG fracturing fluid on different clay minerals. (4) Evaluation of fracturing fluid adsorption through SEM observation. Two-dimensional SEM and three-dimensional AFM observation of rock samples before and after fracturing fluid adsorption.

The evaluation steps for dynamic adsorption capacity and

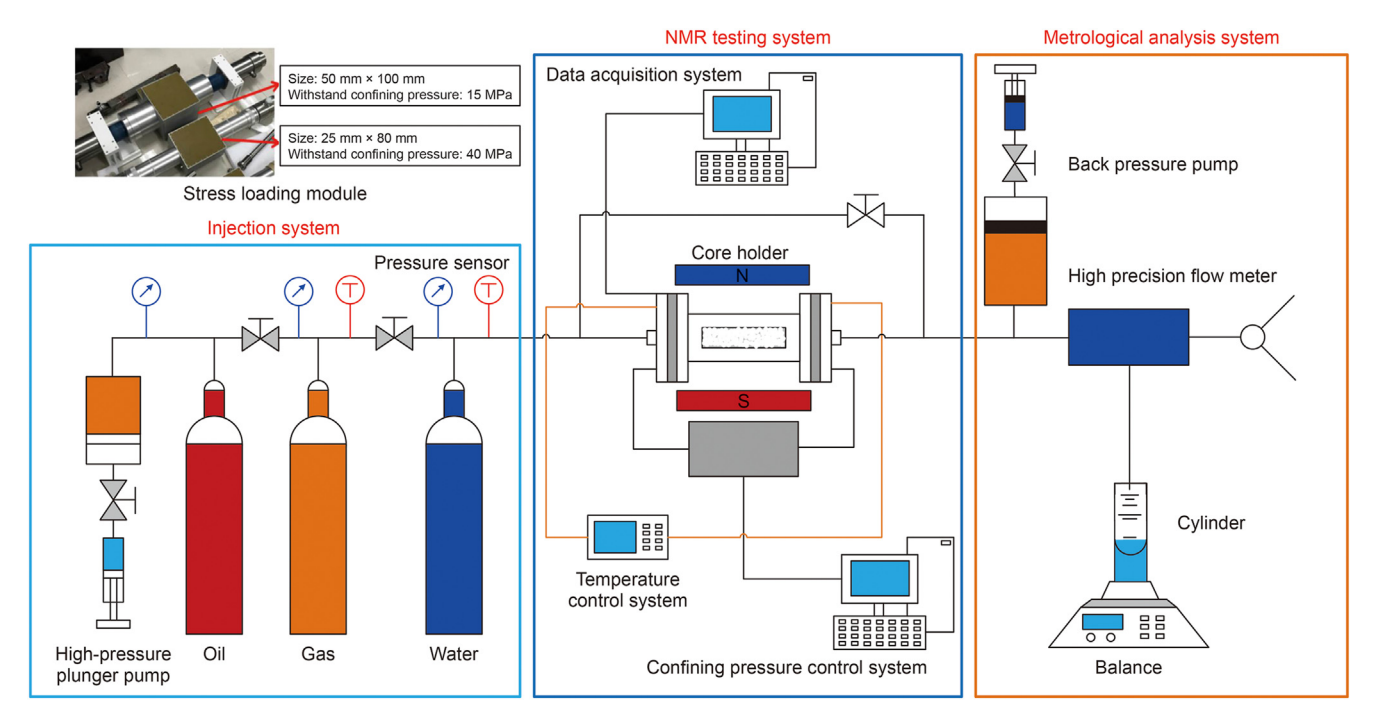


Fig. 2. Schematic diagram of the HTHP core displacement experimental device equipped with on-line NMR test function.

damage degree are as follows: (1) Place the core into the holder and proceed to inject the HPG fracturing fluid into the core with a constant pressure difference. Initiate sampling every 20 min once the liquid flows out from the outlet end. (2) Determine the concentration of the fracturing fluid by measuring absorbance until stability is reached. (3) After 36 min of stabilization, the fluid's dynamic retention can be calculated by determining the concentration after dynamic adsorption stabilization based on absorbance. (4) Conduct permeability testing every 20 min, measure the absorbance, and calculate the dynamic adsorption capacity of the fracturing fluid.

2.2.4. Microscopic analysis of rock-fracturing fluid contact

2.2.4.1. Residue full-size distribution test. Following the breakage of the fracturing fluid gel, the solid residue is divided into both coarse and fine fractions. The coarser fraction is subjected to analysis using a Malvern laser particle sizer, while the finer fraction is analyzed with nano-dynamic laser scattering, as part of the characterization process for the full-size distribution (Kang et al., 2014; Zhang D.J. et al., 2019).

characterization. The 2.2.4.2. Adsorption morphology threedimensional adsorption patterns and adsorbed thickness of HPG fracturing fluid on sandstone surfaces with various minerals were quantitatively characterized using AFM (Eysden et al., 2008). The following steps are required for the experiment: (1) Mosaic and polish the rock fragments, while simultaneously preparing and obtaining the filtrate of HPG fracturing fluid; (2) Immerse the sandstone samples in the fracturing fluid while maintaining the temperature of the formation for 72 h: (3) Rinse the samples with deionized water, then use AFM to observe the three-dimensional adsorption morphology on the rock surface after natural airdrying; (4) Record the thickness of the adsorbed layer on the XY plane and the diagonal of the sandstone surface under varying experimental conditions.

2.2.4.3. SEM observation after fracturing fluid action. SEM is capable of accurately assessing the changes in rock pores and minerals following exposure to fracturing fluid. For SEM analysis, the cores subjected to dynamic damage evaluation after being exposed to fracturing fluid were divided into three sections (front, middle, and back).

3. Results and discussion

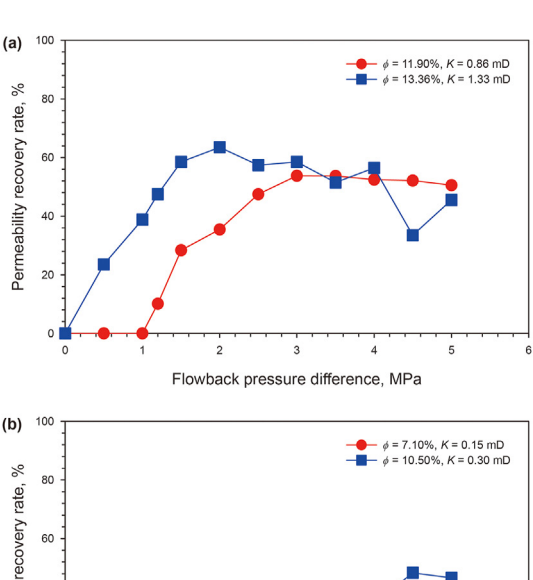
3.1. Comprehensive dynamic damage characteristics of HPG fracturing fluid to the formation

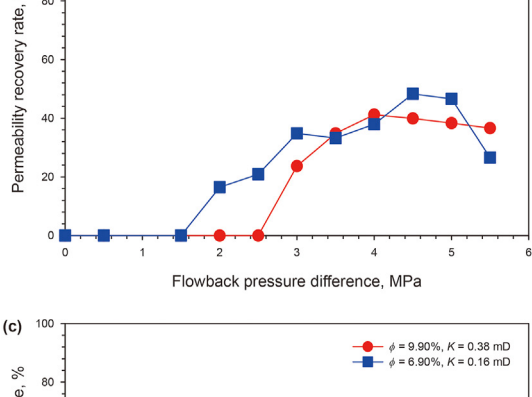
The dynamic damage evaluation results provide a comprehensive depiction of damage induced by fracturing fluids, encompassing solid-phase, liquid-phase, and adsorption damage, alongside various other types. The damage caused by fracturing fluids in tight sandstone containing varying clay minerals is comprehensively illustrated in Table 2 and Fig. 3. The findings suggest that samples with lower core permeability are more susceptible to both dynamic and static damage caused by fracturing fluids. The comparison of dynamic and static damage results for fracturing fluids under identical conditions reveals that the dynamic damage rate is observed to be lower than the static damage rate for LSF and TF rock samples. However, the dynamic damage rate of fracturing fluids in the USF rock samples is slightly higher than their static damage rate. This implies that the damage pattern in LSF and TF is primarily characterized by liquid-phase damage, whereas USF may experience solid-phase damage due to the invasion of fracturing fluid residue and fines.

To investigate the solid-phase damage of fracturing fluids on gas transport in tight sandstone with different clay minerals, a comparison between residue particle size and rock pore throat size was conducted. The solid residue was separated into coarse and fine fractions subsequent to the fracturing fluid gel being broken. Fig. 4 displays the results of the residue particle size analysis. The coarse fractions measured by the Marvin laser particle size analyzer

Table 2Permeability recovery results after dynamic and static damage of fracturing fluid.

Type	Sample	Porosity, %	Permeability, mD	Irreducible water saturation, %	Dynamic permeability damage rate, %	Static permeability damage rate, %
USF	U-1	13.36	1.33	40.87	36.50	28.46
	U-2	11.90	0.86	63.54	46.22	42.74
LSF	L-1	10.50	0.30	47.63	51.70	57.59
	L-2	7.10	0.15	52.67	58.80	64.85
TF	T-1	9.90	0.38	63.59	53.10	57.51
	T-2	6.90	0.16	66.97	64.60	66.55





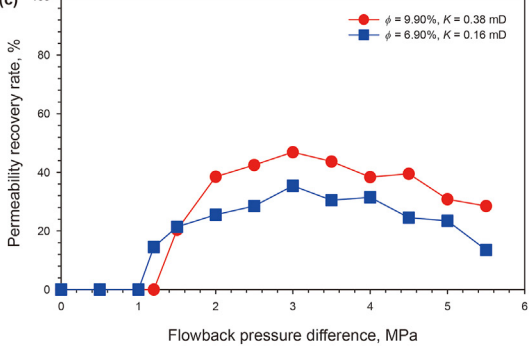


Fig. 3. Permeability recovery rate after fracturing fluid dynamic damage of variable pressure differential displacement in different gas layers: (a) USF; (b) LSF; (c)TF.

revealed D_{50} and D_{90} values of 33.03 and 83.07 µm, respectively. The fine fractions, on the other hand, were measured through dynamic light scattering and had D_{50} and D_{90} values of 1.83 and 3.66 µm, respectively. After comparing the pore size distribution of the three types of gas formations (maximum pore throat radius ranges from 1.137 to 1.948 µm) (Zhang et al., 2020), it is suggested by the D_{90} rule that solid-phase residues in the fine fraction of fracturing fluid may invade pores and cause solid-phase damage (Wang et al., 2021), while those in the coarse fraction run a risk of

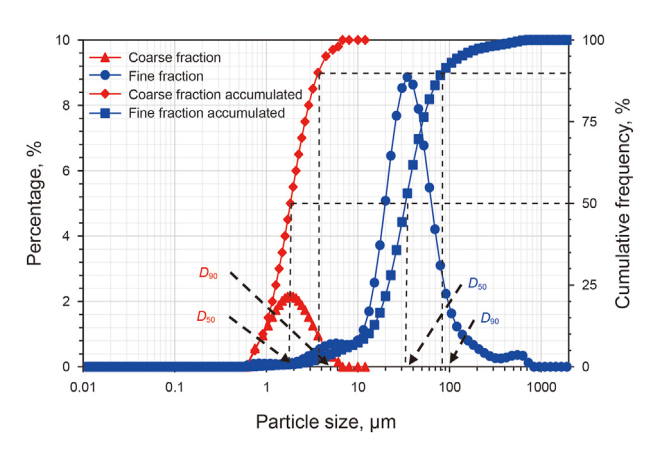


Fig. 4. Full-size distribution of fracturing fluid residue.

clogging proppant gaps (based on the 40/70 mesh ceramic grains). Comparatively, LSF and TF samples exhibit narrower pore throats, which poses challenges for the finer fraction of the fracturing fluid to infiltrate these pore throats. As a result, dominant liquid phase damage occurs in the fracturing fluid while solid phase damage is weak or almost negligible. This suggests that the filter cake formed by dynamic cyclic shear of the fracturing fluid partially impedes continuous infiltration of solid residue particles, HPG macromolecules, and the filtrate of the fracturing fluid (Kang et al., 2014).

The microstructural changes of clay minerals were analyzed using SEM analysis on the front, middle, and back end faces of the cores after conducting dynamic damage evaluation experiments. Fig. 5(a) shows the injection end of the core after the action of HPG fracturing fluid. Observations reveal that the surface of the rock grains and pores are heavily contaminated, with flocculent residues, particles, and crystallised salts adhering to the surfaces or filling in the pore spaces. This resulted in substantial blockage of the pores, which was evident by magnifying the SEM image (Fig. 5(b)). In the middle region (about 2.5 cm), it can still be observed that some residues and fines cause blockage. Moreover, the intergranular pores exhibit a surface coverage of both flocculent material and a membrane film composed of polymers (Fig. 5(c)). At the exit end of the core (> 4 cm), the grain surface appears rather clean and the microstructure of the clay minerals is well maintained, but some of the ammonium interlayer minerals adsorbed by the fracturing fluid become flocculent (Fig. 5(d)).

During the process of fracturing, as shear and pressure differentials cause the invasion of fracturing fluid into the matrix, a majority of residues and polymers are primarily mechanically retained near the fracture face at the inlet end of the pore space (Fig. 6(a) and (b)). The extent of solid-phase damage decreases with decreasing size and quantity of retained residues and polymers at deeper locations. The invasion depth of solid particles is correlated with the pore throat size of the formation. The smaller the pore throat size of the matrix, the shallower the invasion depth of the solid phase. Research has demonstrated that due to capillary forces

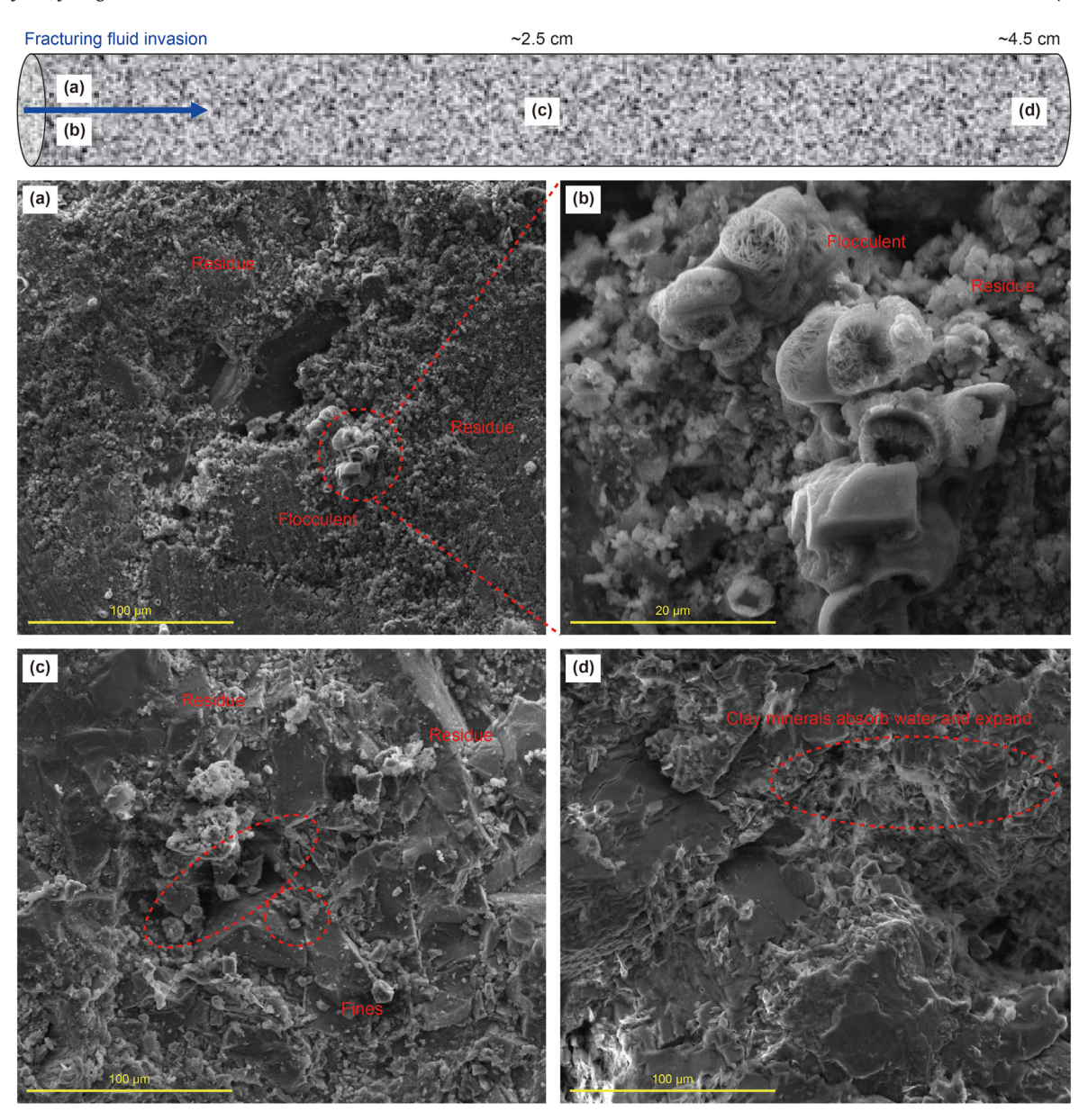


Fig. 5. SEM observation results of the front, middle, and back end faces of the core after dynamic fracturing fluid damage experiments: (a) injection end of the core; (b) enlarged result of the red dashed circle in image (a); (c) middle region of the core; (d) exit end of the core.

and pressure differentials, the liquid phase exhibits significantly greater invasion depth compared to the solid phase (Kang et al., 2014). At the core outlet, the adsorption of fracturing fluid onto clay minerals is evident, resulting in the expansion of clay crystals and a transformation in the microstructure of clay minerals from bridging to thin film and flake-like morphology (Fig. 6(c) and (f)). The clay minerals in LSF samples are mainly kaolinite, which has a large specific surface area. The polymer adheres to the mineral surfaces, resulting in the formation of inclusions that obstruct both suture surface pores and intergranular pores (Fig. 6(d) and (e)). The TF rock samples are primarily dominated by illite minerals. A substantial quantity of polymers and particles adhere to the surface of the clay mineral crystals. The adhesion between mineral crystals leads to their coarsening, resulting in the formation of fibrous short columnar particles that are approximately 1-2 µm thicker than their initial state (Fig. 6(g) and (h)). The application of fracturing fluid on the surface of the grains induced a directional arrangement

by causing filamentous illite to undergo bending. The fracturing fluid, upon adsorption by filamentous illite, effectively obstructed and enveloped the intercrystalline micropores, inducing a transformation in the microstructure of clay minerals from a hair-like, bridged morphology to a dispersed thin film and flake-like structure. During gas displacement flowback of the fracturing fluid, numerous previously absorbed illite minerals underwent fragmentation into short fiber columns and crystal fragments. These fragments were subsequently randomly accumulated within the intergranular space or on the grain surface, ultimately resulting in blockage of intergranular pores (Fig. 6(i)).

3.2. Fracturing fluid filtrate retention distribution and its effect on WPT damage

To further investigate the spatial distribution of retained fracturing fluid filtrate in the pore space and its impact on WPT

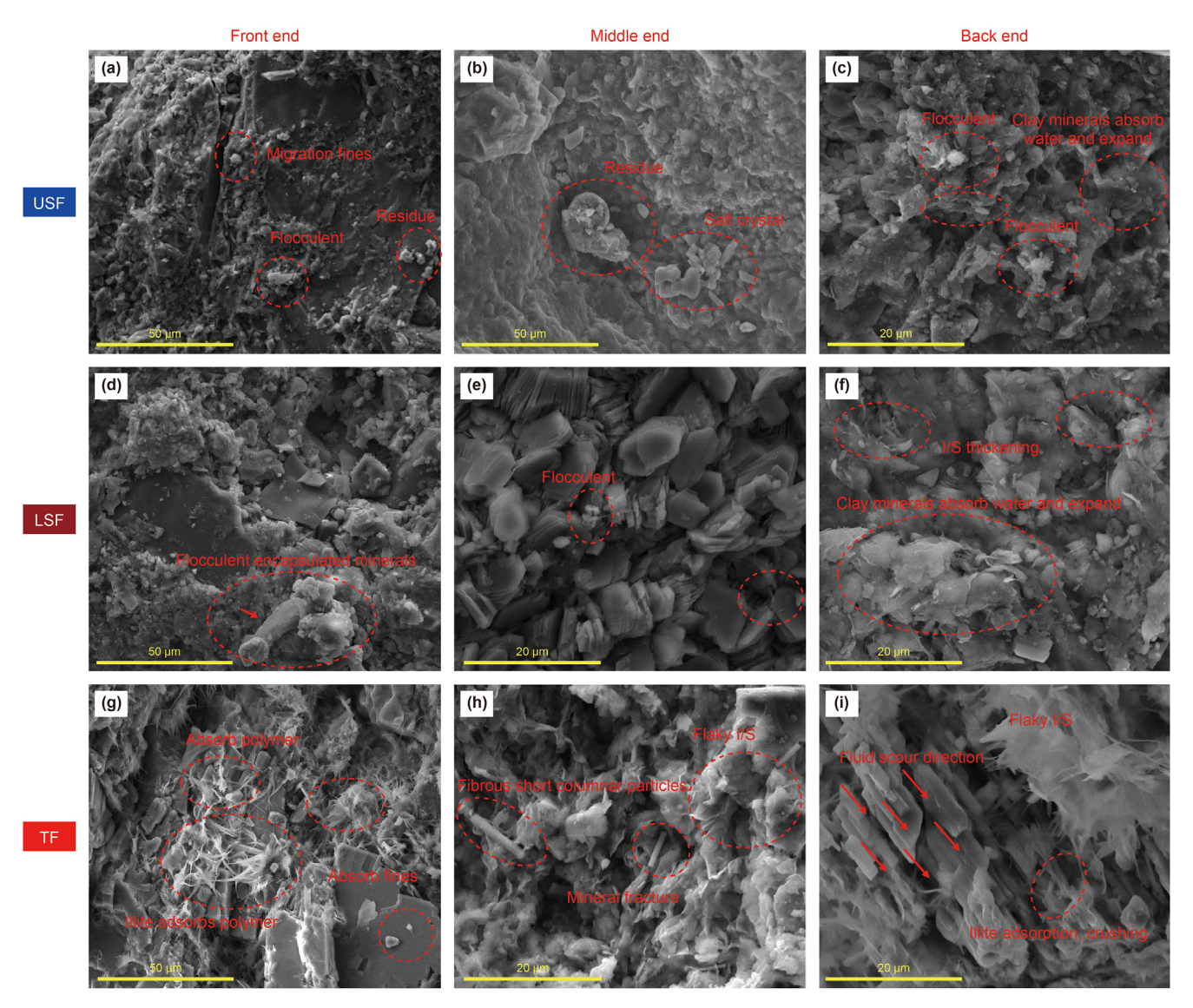


Fig. 6. SEM results of fracturing fluid damage in different clay minerals: (a) residues and polymers retained; (b) residue and salt crystal blocking the pores; (c) absorption of fracturing fluid onto clay minerals and microstructure change; (d) flocculent encapsulated minerals; (e) flocculent blocking the suture surface pores; (f) adsorption of fracturing fluid onto illite/smectite; (g) illite adsorption of polymer onto illite; (h) illite converted to fibrous short columnar; (i) illite adsorption, crushing.

damage, on-line NMR tests were conducted during gas displacement. The water volume profiles during gas displacement under constant differential pressure are illustrated in Fig. 7. The findings depicted in Fig. 7 demonstrate a pronounced tendency for the gas phase to rapidly establish a seepage pathway, gradual reduction of NMR signal volume, and discontinuous distribution trend of the water phase with increasing gas displacement time. Following the establishment of the gas-phase preferential flow pathway, the volume of fracturing fluid filtrate flowback reduces continuously. The majority of the fracturing fluid in the pore space ranging from 0.1 to 1 µm is challenging to flowback, leading to the formation of irreducible fluid (You et al., 2019). Samples with relatively low permeability (K < 0.5 mD) encounter challenges in overcoming the high capillary resistance of small pores under constant differential pressure displacement. Consequently, the stronger preferential flow pathway effect leads to increased retention of fracturing fluid after gas displacement flowback (Fig. 7(c) and (f)).

The effective utilization of fracturing fluid retention in the coarse pore throat can be further enhanced when employing incremental differential pressure for flowback (Fig. 8(b) and (d)).

However, some of the fracturing fluid discharged from the coarse pore throat ($T_2 > 50 \text{ ms}$) during flowback may become trapped due to seepage in the fine pore throat, leading to a tendency for increased accumulation of fracturing fluid within certain fine pore throats ($T_2 < 50$ ms) (Fig. 8(c) and (f)). When comparing the performance of different permeabilities, it becomes apparent that samples with relatively lower permeability demonstrate a higher discharge of fracturing fluid during stepwise incremental differential pressure displacement. Moreover, the implementation of incremental differential pressure driving can significantly enhance the flowback rate of samples characterized by relatively low permeability, particularly for expelling fracturing fluid from submicron pore throats (0.1–1 μm). The proportion of large pores is higher than that of small pores in the samples with relatively high permeability (K > 0.5 mD), and the fracturing fluid can be discharged from the large pores with either constant or increasing differential pressure (Fig. 9). The presence of small pores in samples with relatively low permeability often hinders the complete discharge of fracturing fluid from larger pores under low differential pressures. To enhance the rate of fracturing fluid flowback, a

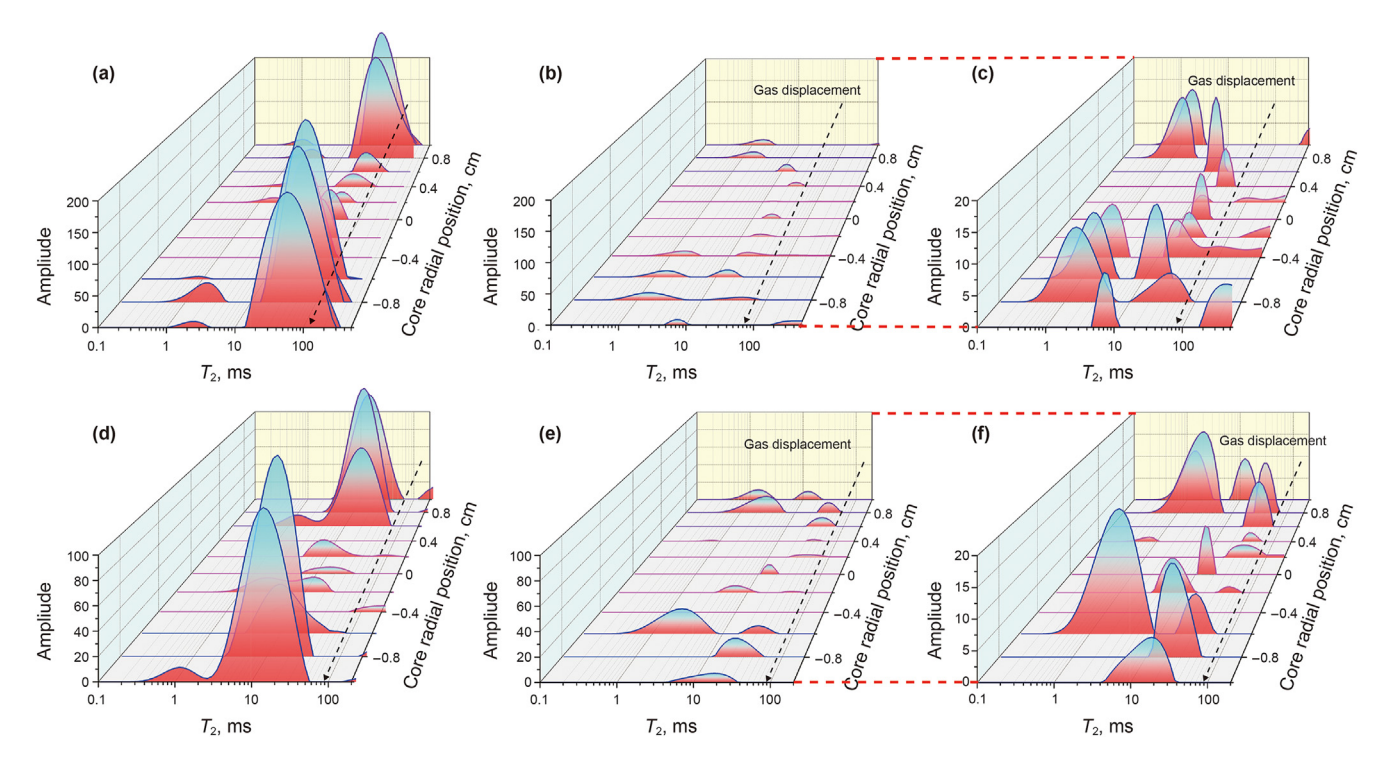


Fig. 7. One-dimensional water volume profiles during gas displacement under constant differential pressure: (**a**) relatively high permeability, before displacement; (**b**) after displacement; (**c**) enlarged results of (b); (**d**) relatively low permeability, before displacement; (**e**) after displacement; (**f**) enlarged results of (e).

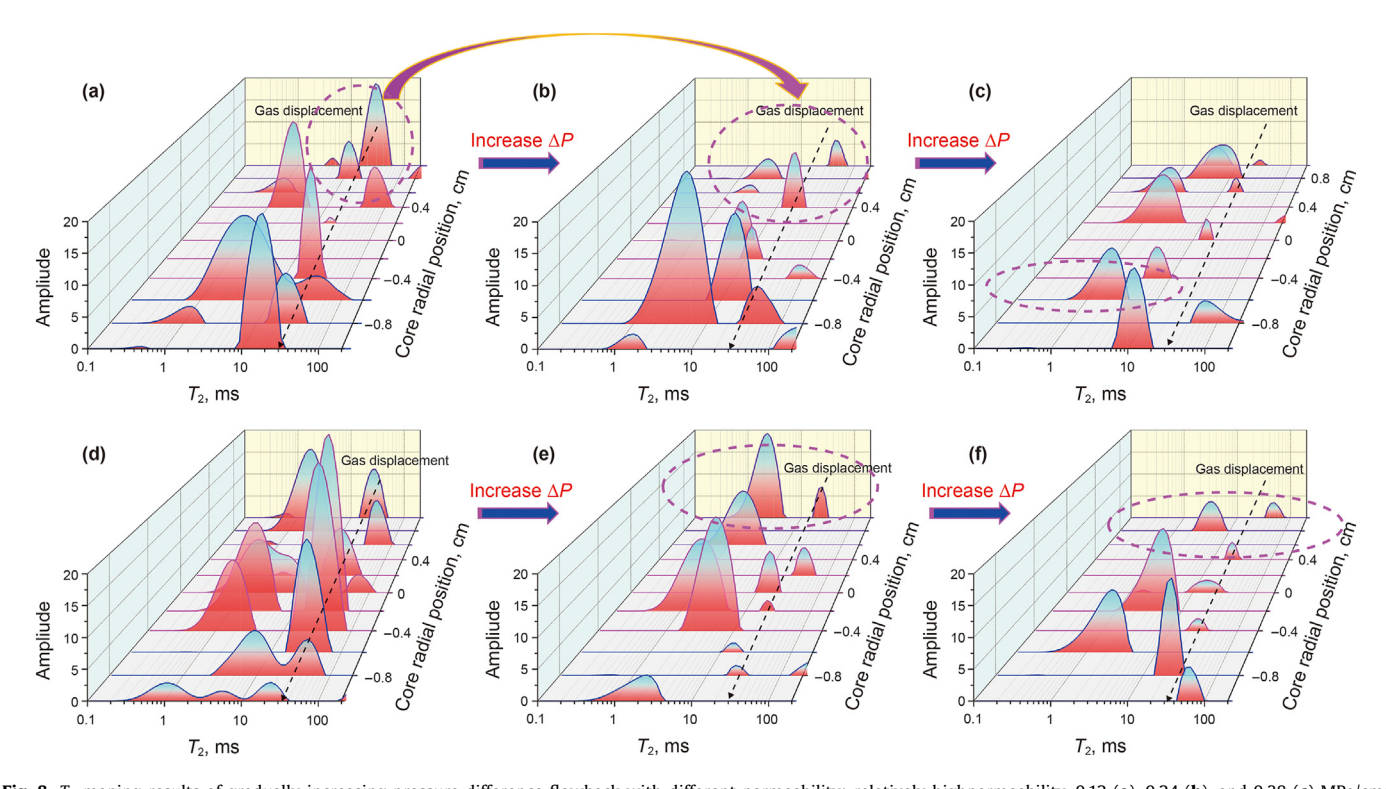


Fig. 8. T_2 maping results of gradually increasing pressure difference flowback with different permeability: relatively highpermeability, 0.12 (**a**), 0.24 (**b**), and 0.38 (**c**) MPa/cm; relatively low permeability, 0.12 (**d**), 0.24 (**e**), and 0.38 (**f**) MPa/cm.

gradual increase in differential pressure can be implemented.

The recovery of gas-phase permeability at the exit end of the flowback stage was tested in parallel with the on-line NMR monitoring of the spatial and temporal evolution of the fracturing fluid distribution (Fig. 10). For the relatively hypertonic samples (K > 0.5 mD), the irreducible water saturation is in the range of 31.53%—41.47%, and the rate of permeability damage varies between 36.58% and 43.54%. In the case of relatively hypotonic samples (K < 0.5

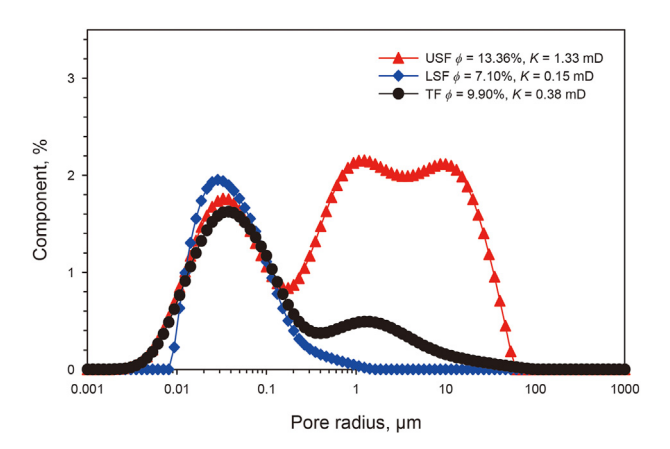
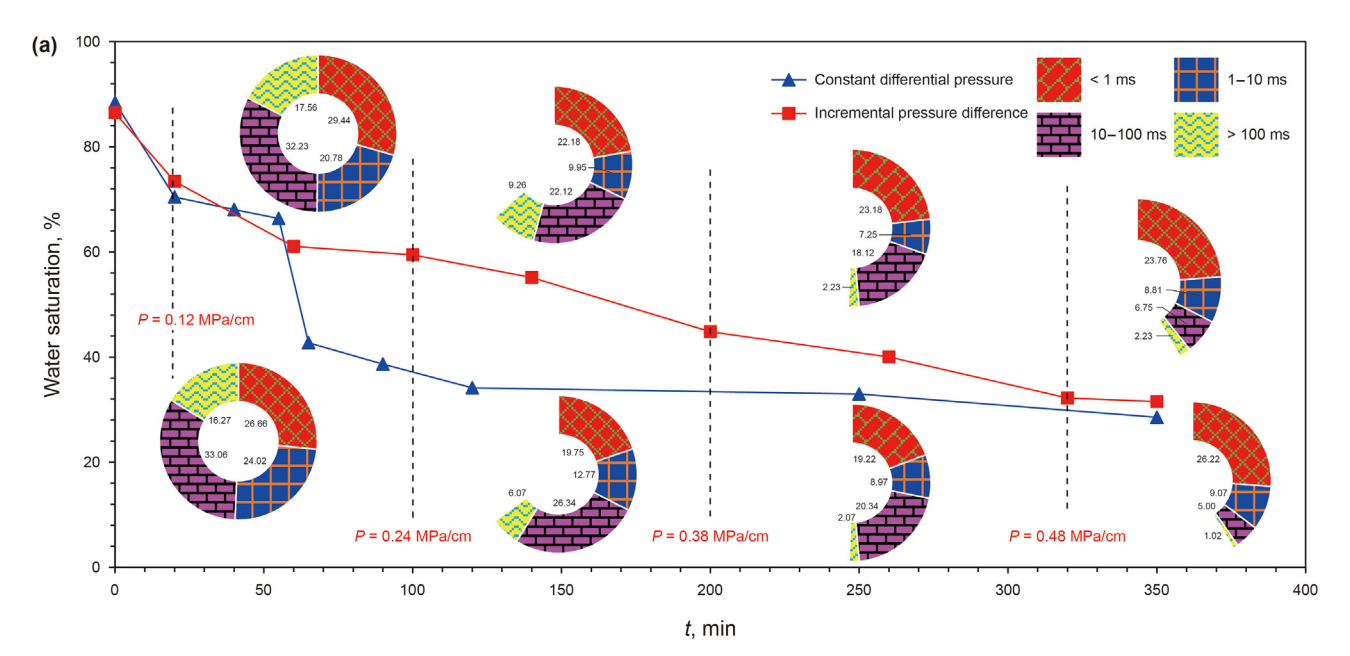


Fig. 9. Comparison results of pore size distribution of different physical properties.

mD), the irreducible water saturation ranged from 39.53% to 55.80%, whereas the permeability damage rate span from 58.35% to 65.89% (Fig. 10). There are slight variations in the irreducible water saturation levels between the relatively hypertonic and hypotonic samples. However, there is a significant difference in the gas-phase permeability damage rate. A notable dissimilarity exists in the recovery capacity of gas phase permeability due to the differing distribution of retained fracturing fluid (Fig. 11). The NMR SE imaging results indicate that sandstone samples with good physical properties (K > 0.5 mD) have a scattered distribution of retained fracturing fluid (Fig. 11(a) and (b)). The majority of gas phases interconnect to create a continuous and stable seepage pathway, resulting in a high gas-phase permeability recovery rate at a macroscopic level and a high yield gas well. On the contrary, samples with relatively poor physical properties (K < 0.5 mD) exhibit weak NMR signals. The fracturing fluid is distributed as a



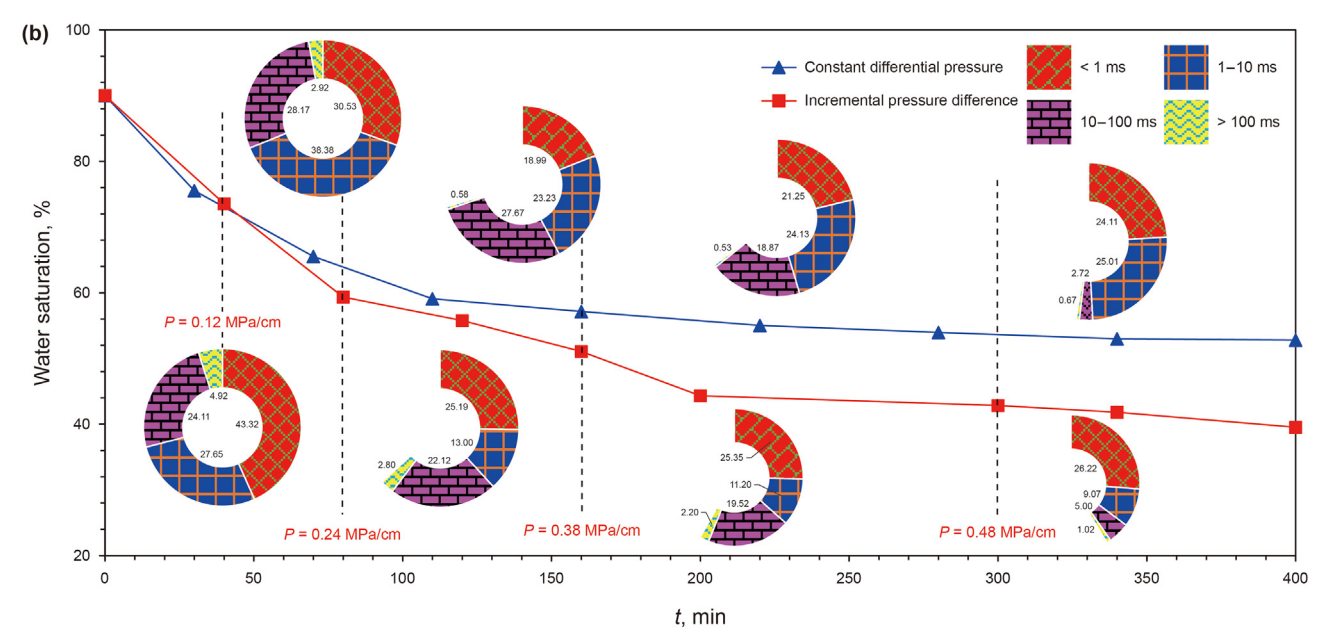


Fig. 10. Changes in water saturation of tight sandstones with different permeability under different flowback methods: (a) relatively high permeability (Samples U-1 and U-2); (b) relatively low permeability (Samples T-1 and T-2).

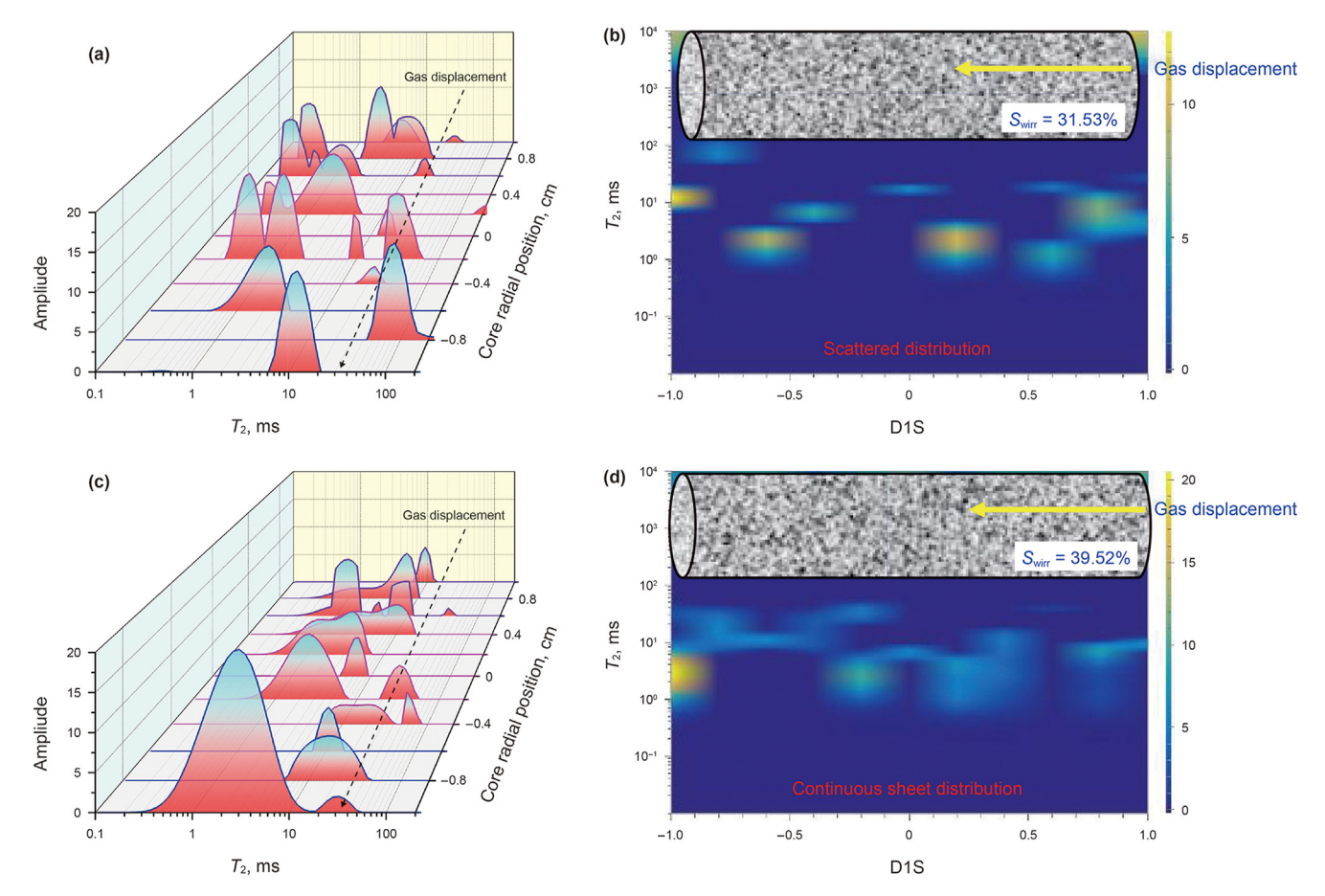
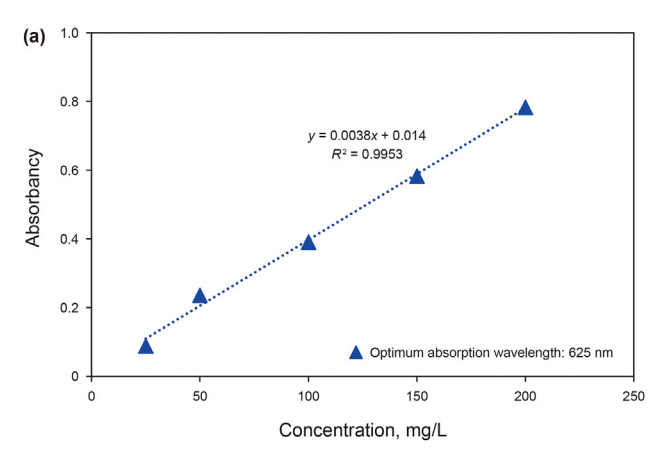


Fig. 11. Distribution of detention fracturing fluids for tight sandstones with different permeability: relatively high permeability, stratified T_2 spectrum results (**a**) and SE visualization results (**b**); relatively low permeability, stratified T_2 spectrum results (**c**) and SE visualization results (**d**).

continuous sheet, resulting in the entrapment of a significant amount of gas within the water phase, thereby impeding its flow (Fig. 11(c) and (d)). Consequently, gas wells suffer from low production. This highlights the need to effectively prevent and control WPT damage while developing gas reserves with inferior physical properties.

3.3. Adsorption damage characteristics of fracturing fluid in tight sandstones with different clay minerals

The static damage induced by fracturing fluid filtrate exhibits a



distinct deviation from the damage rate of WPT in parallel formation water with equivalent physical properties. This indicates that static damage caused by fracturing fluid includes not only WPT damage but also adsorption damage (Li et al., 2022; Xu et al., 2020). The static adsorption results of distinct clay mineral tight sandstone in contact with fracturing fluid are presented in Fig. 12. The saturated adsorption amounts of USF, LSF, and TF fracturing fluid were 2.587, 2.735, and 2.858 mg/g, respectively. The experimental results demonstrate that the adsorption of HPG fracturing fluid on sandstone rock conforms to both Langmuir and Freundlich adsorption isotherms. Based on the coefficient of fit, it is evident that

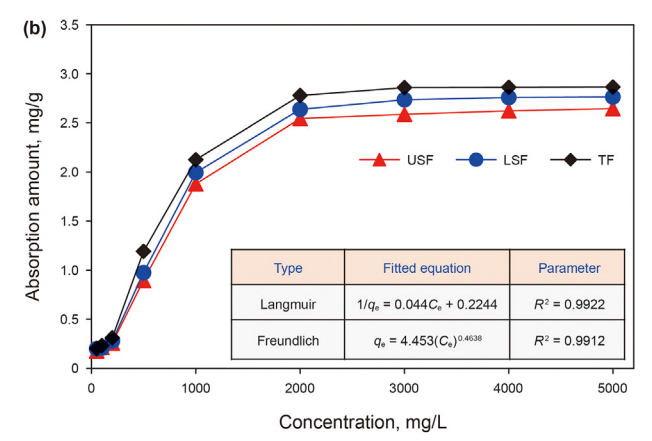
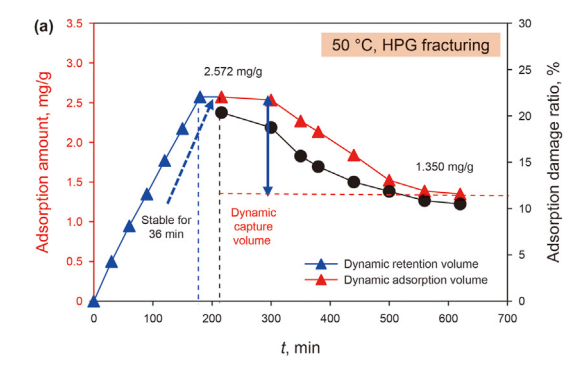
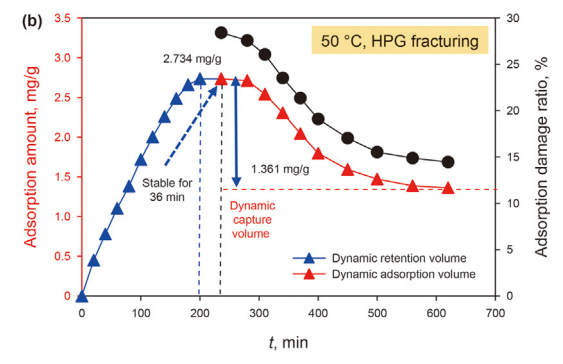


Fig. 12. Evaluation results of static adsorption of fracturing fluid on tight sandstone with different clay minerals: (a) adsorption standard curve; (b) static saturated adsorption capacity and interpretation results of Langmuir and Freundlich models.

adsorption is primarily physical adsorption (Fig. 12(b)). Following the contact reaction between the rock and the fracturing fluid, a SEM observation was conducted on the sample that had been frozen with nitrogen. The results are illustrated in Fig. 13, which revealed a destruction in the network structure of the fracturing fluid caused by adsorption. The primary factor for the formation of residue was determined as the entanglement and accumulation of polymer after the destruction of the fluid. The dynamic adsorption capacity of USF, LSF, and TF fluids was determined to be 1.350, 1.361, and 2.075 mg/g, respectively (Fig. 14). Additionally, during the flowback stage of gas displacement, dynamic gas flow caused a partial desorption of adsorbed fracturing fluids. The percentage of dynamic adsorption that could be desorbed from USF, LSF, and TF was observed to be 47.51%, 50.21%, and 27.32%, respectively. Most of the fracturing fluids adsorbed in the illite mineral-rich TF samples proved arduous to discharge, a finding endorsed by SEM results (Fig. 6(g) and (h)). A significant quantity of fracturing fluid was adsorbed and retained in the formation, causing dynamic adsorption damage of 10.49%, 14.46%, and 18.74% to USF, LSF, and TF, respectively (Fig. 14).

The AFM analysis was employed to determine the thickness and three-dimensional morphology of adsorbed layers comprising various clay minerals co-adsorbed with the fracturing fluid (Fig. 15). The adsorption of fracturing fluid in both USF and LSF exhibited "needle tip" or "column" patterns, whereas in sandstone of TF, it showed "flake" or "band" patterns. The absorption patterns of fracturing fluids are linked to the types of minerals, contents, and intermolecular aggregation effects. The thickness of the adsorbed layer of tight sandstone with different clay minerals in contact with the fracturing fluid is shown in Fig. 16. The average thicknesses of the adsorbed layers for USF, LSF, and TF were 12.11, 20.60, and 34.06 nm, respectively. Typically, monolayer adsorption is assumed when the thickness of the adsorbed layer falls within the range of 0–5 nm; bilayer adsorption occurs when the thickness is between 5 and 10 nm; and multilayer adsorption takes place when the thickness exceeds 10 nm (Guo et al., 2018a). The sandstones in the USF and LSF primarily undergo monolayer and bilayer adsorption, whereas the TF predominantly experiences multilayer adsorption. The expansive surface area and presence of filamentous illite minerals facilitate the multiple winding and adsorption of fracturing fluids. After the adsorption of fracturing fluid by the filamentous illite mineral, a significant amount of fracturing fluid fills the intergranular micropores of the mineral (Figs. 15 and 6). The guar gum molecular chains which have previously been adsorbed





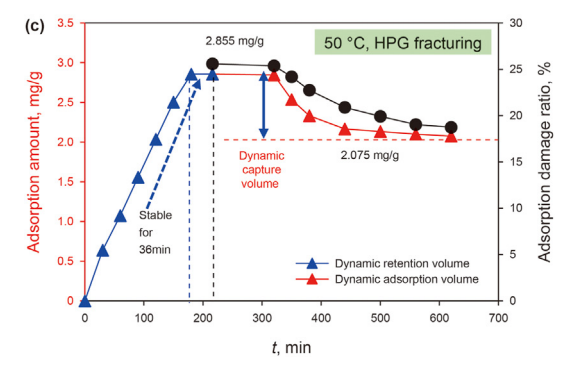
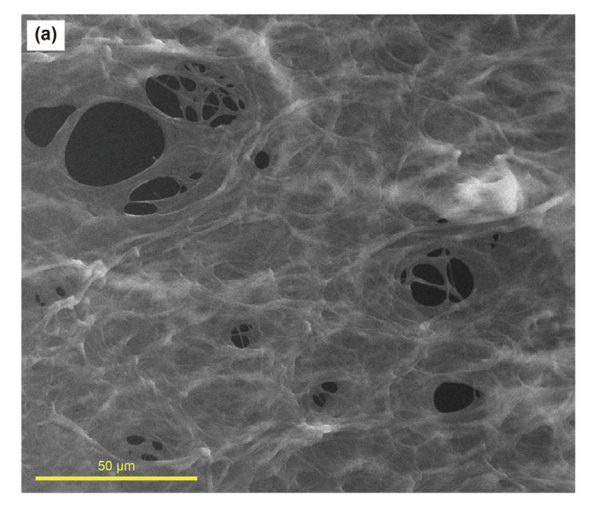


Fig. 14. Evaluation results of dynamic adsorption of fracturing fluid on tight sandstone with different clay minerals: (a) USF; (b) LSF; (c) TF.

on the rock surface encounter the widely dispersed guar gum molecules within the solution, establishing formidable



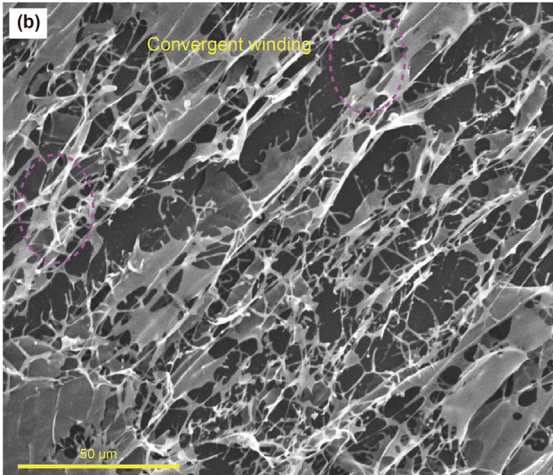


Fig. 13. SEM observation results before (a) and after (b) the contact reaction between fracturing fluid and rock. (a) shows before contact reaction, the fracturing fluid has a network structure; and (b) indicates the network structure is damaged after contact reaction.

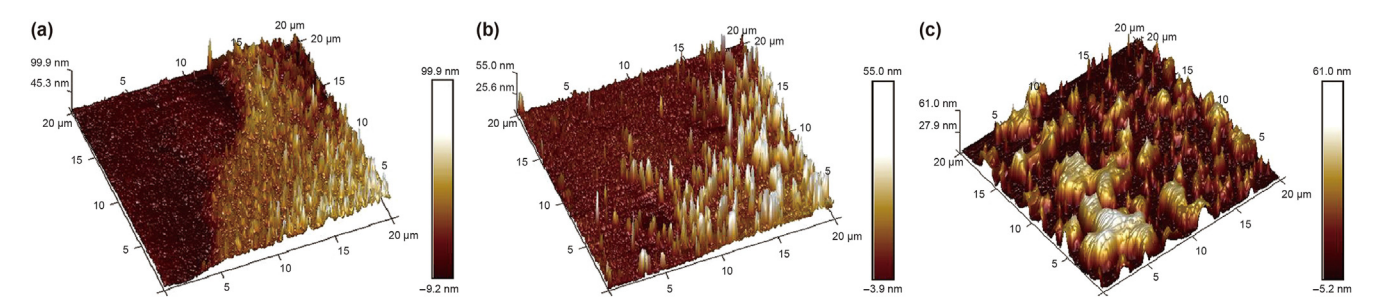


Fig. 15. Three dimensional adsorption morphology results of tight sandstone with different clay minerals treated with fracturing fluid: (a) USF; (b) LSF; (c) TF.

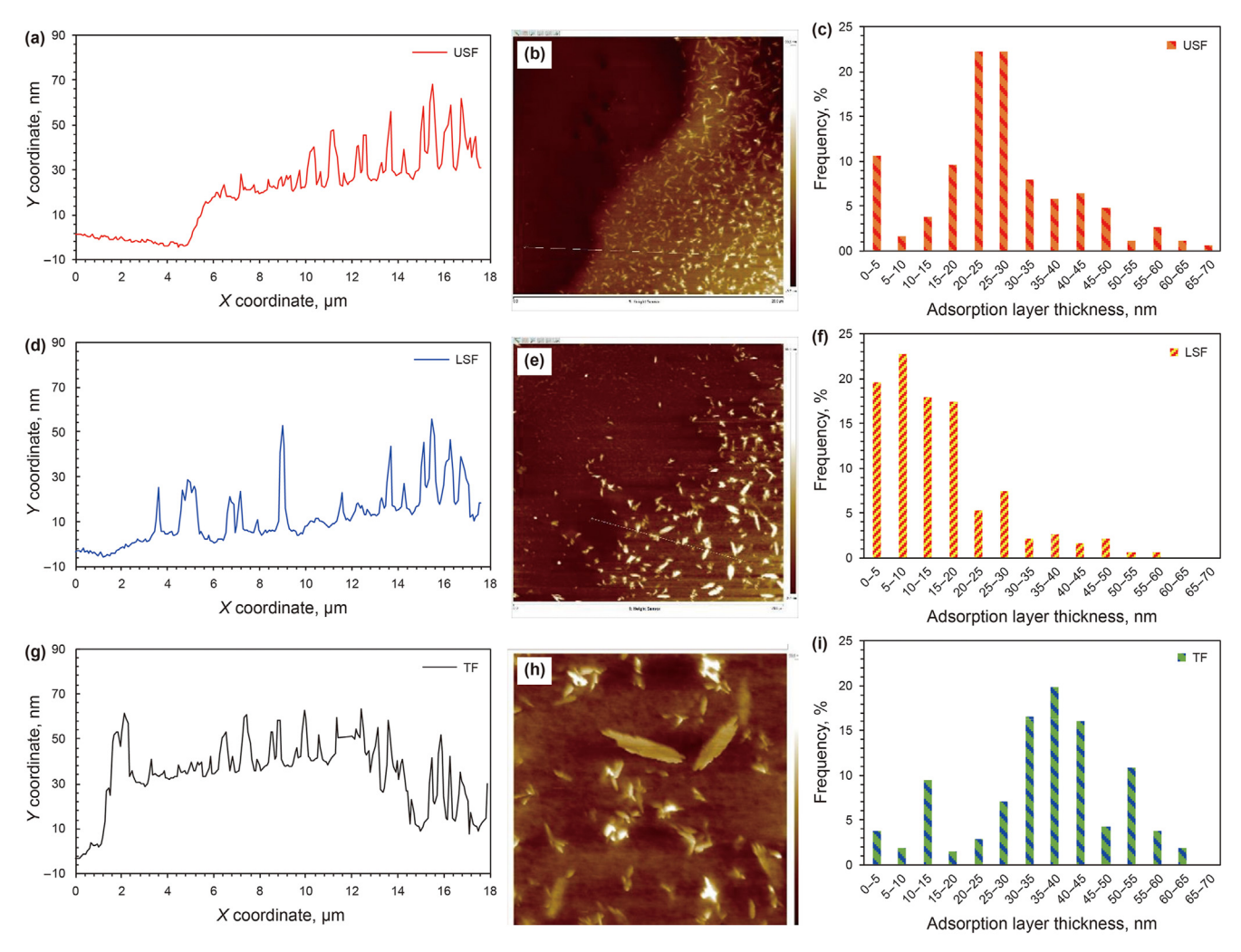


Fig. 16. Thickness of adsorption layer after fracturing fluid treatment of tight sandstone with different clay minerals: adsorption thicknesses of USF (**a**), LSF (**d**), and TF (**g**); adsorption morphology of USF (**b**), LSF (**e**), and TF (**i**).

intermolecular hydrogen-bonding. Consequently, the former are ascertained to be "stably" adsorbed on the rock surface, which exhibits a multi-layered adsorption characteristic.

4. Implications for formation damage control of tight sandstone with different clay minerals while fracturing

The geological characteristics of the reservoir in the study block are complex, involving a vertical development of multiple gas formations (Zhang et al., 2020). The simultaneous hydraulic fracturing

of multiple formations is often necessary for the advantageous development of these formations (Tan et al., 2023). However, the gas formations exhibit significant diversity in terms of rock properties, encompassing a wide range of clay mineral types and compositions. Consequently, the interaction between the fracturing fluid and formation rock inevitably leads to formation damage. Chlorite is the primary clay mineral present in the USF, and the physical properties of the formation are favorable (Table 3). The formation exhibits a high proportion of large pores and coarse throat, leading to a low threshold pressure. WPT damage is the

Table 3

 Permeability damage results of fracturing fluid to different clay minerals.

Layer	Main clay type	Solid-phase damage, %	Static permeability damage, %	WPT damage, %	Adsorption damage,%
USF	Chlorite	36.50-46.22	28.46-42.74	36.58-43.54	10.49
LSF	Kaolinite	51.70-58.80	57.59-64.85	58.35-63.36	14.46
TF	Illite	53.10-64.60	57.51-66.55	61.26-65.89	18.74

dominant form of fracturing fluid damage, followed by solid-phase damage. Adsorption damage is comparatively weaker in comparison. The primary clay mineral present in LSF is kaolinite, with notable inadequacies in the formation's physical properties and well-developed intercrystalline pores. The fracturing fluid-induced damage is primarily dominated by WPT damage, followed by adsorption damage, while solid-phase damage remains comparatively weak. The primary clay mineral in TF sandstone is illite, which exhibits poor physical properties and a high threshold pressure. WPT damage is the dominant type of damage, followed by fracturing fluid adsorption damage.

The geological characteristics of the main gas formations exhibit substantial variation, and the severity of fracturing fluid damage also displays a variable sequence. Consequently, it is imperative to employ more targeted damage prevention and control measures when conducting hydraulic fracturing (Xu et al., 2020; Fu et al., 2020). The primary objective for optimizing fracturing fluid in the context of the USF should be to enhance operational efficiency and facilitate effective flowback, thereby controlling and preventing water-sealed gas. Additionally, reducing the residue content, fines size, and molecular quality of the fracturing fluid from the perspective of the amount of gel breaker used may help to mitigate the negative effects of solid-phase plugging. For LSF and TF, the optimization of fracturing fluids also aims to minimize the damage caused by WPT. However, in contrast to USF, LSF and TF exhibit inferior physical properties. This makes it challenging for cleanup agent to penetrate tiny pores to be effective. As a result, LSF and TF must explore novel approaches to prevent the gas phase from being blocked by the bulk water phase. To fill the gap, we are conducting research to inject CO₂ or N₂ microbubbles into gas reservoirs to relieve the WPT damage. The main idea is to use the special properties of micro-nano bubbles to quickly cross the channels occupied by the aqueous phase, to realize the communication with the gas phase at the far end, and to establish a channel for gas phase seepage. This part of the research work has now gained initial insights, so stay tuned for subsequent reports on the results. Furthermore, it is recommended that LSF and TF concentrate on reducing the thickness of the adsorption layer of thickeners in fracturing fluid. This can be achieved by coordinating competitive adsorption mechanisms to weaken the adsorption capacity of the thickeners.

5. Conclusions

In this study, we investigated the damage characteristics of fracturing fluids in tight sandstone gas formations consisting of three types of clay minerals, utilising on-line NMR, AFM, and SEM. Our findings indicate that the depth and extent of solid phase damage are determined by the ratio between the size of residual fracturing fluid and the size of rock pore-throat. USF layers with favorable physical properties and larger average pore-throat radius exhibit higher susceptibility to solid phase damage, whereas LSF and TF layers with unfavorable physical properties demonstrate weaker solid phase damage.

In terms of WPT damage caused by fracturing fluid, we have obtained compelling evidence indicating that poor physical properties result in a more pronounced preferential flow pathway effect during flowback. Direct experiments demonstrate that the variation in the distribution of retained fracturing fluid significantly impacts permeability. Favorable physical properties characterized by a scattered distribution of retained fracturing fluid exhibit high gas phase recovery permeability, whereas unfavorable physical properties featuring a continuous sheet-like distribution show low gas phase recovery permeability.

The adsorption characteristics of fracturing fluid in different clay mineral formations vary significantly. The expansive surface area and presence of filamentous illite minerals facilitate the intricate winding and adsorption of fracturing fluids, showcasing robust hydrogen-bonding, multi-layering, and multiple adsorption properties.

The geological characteristics of the main gas formations exhibit significant variation, and the severity of fracturing fluid damage also varies. To address this issue, we propose a differentiated strategy for optimizing fracturing fluids that incorporates innovative methods to mitigate well productivity impairment.

CRediT authorship contribution statement

Yi-Jun Wang: Writing — original draft, Methodology, Investigation, Data curation. **Li-Jun You:** Writing — review & editing, Resources, Project administration, Conceptualization. **Jian Yang:** Validation, Supervision, Data curation. **Yi-Li Kang:** Writing — review & editing, Supervision, Resources. **Ming-Jun Chen:** Writing — review & editing, Visualization, Validation, Conceptualization. **Jia-Jia Bai:** Writing — review & editing, Software, Resources. **Jian Tian:** Writing — review & editing, Writing — original draft, Methodology, Investigation, Formal analysis, Data curation, Conceptualization.

Declaration of competing interest

The authors declare that they have no known competing financial interests or personal relationships that could have appeared to influence the work reported in this paper.

Acknowledgements

This work was supported by the Sichuan Youth Science and Technology Innovation Research Team Project (No. 2021JDTD0017), and the open Fund (PLN2022-11) of State Key Laboratory of Oil and Gas Reservoir Geology and Exploitation (Southwest Petroleum University), and Southwest Petroleum University Graduate Innovation Fund (No. 2022KYCX021). Jian Tian would like to acknowledge the funding from the National Natural Science Foundation of China (52404023).

References

Anderson, A., Rezaie, B., 2019. Geothermal technology: trends and potential role in a sustainable future. Appl. Energy 248, 18–34. https://doi.org/10.1016/j.apenergy.2019.04.102.

Bai, J., Kang, Y., Chen, M., Liang, L., You, L., Li, X., 2019. Investigation of multi-gas transport behavior in shales via a pressure pulse method. Chem. Eng. J. 360, 1667–1677. https://doi.org/10.1016/j.cej.2018.10.197.

Cai, J., Li, C., Song, K., Zou, S., Yang, Z., Shen, Y., et al., 2020. The influence of salinity a

mineral components on spontaneous imbibition in tight sandstone. Fuel 269, 117087. https://doi.org/10.1016/j.fuel.2020.117087.

- Cai, J., Jin, T., Kou, J., Zou, S., Xiao, J., Meng, Q., 2021. Lucas—Washburn equation-based modeling of capillary-driven flow in porous systems. Langmuir 37 (5), 1623—1636. https://doi.org/10.1021/acs.langmuir.0c03134.
- Chitrala, Y., Moreno, C., Sondergeld, C., Rai, C., 2013. An experimental investigation into hydraulic fracture propagation under different applied stresses in tight sands using acoustic emissions. J. Petrol. Sci. Eng. 108, 151–161. https://doi.org/10.1016/j.petrol.2013.01.002.
- Eysden, C., Sader, 2008. Frequency response of cantilever beams immersed in viscous fluids with applications to the atomic force microscope: arbitrary mode order. J. Appl. Phys. 101 (4), 1–11. https://doi.org/10.1063/1.368002.
- Fu, L., Liao, K., Ge, J., Huang, W., Chen, L., Sun, X., Zhang, S., 2020. Study on the damage and control method of fracturing fluid to tight reservoir matrix. J. Nat. Gas Sci. Eng. 82, 103464. https://doi.org/10.1016/j.jngse.2020.103464.
- Guo, J., He, C., 2012. Microscopic mechanism of the damage caused by gelout process of fracturing fluids. Acta Pet. Sin. 33, 1018–1022. https://doi.org/10.7623/syxb201206013 (in Chinese).
- Guo, J., Li, Y., Wang, S., 2018a. Adsorption damage and control measures of slick-water fracturing fluid in shale reservoirs. Pet. Explor. Dev. 45 (2), 320–325. https://doi.org/10.1016/S1876-3804(18)30037-5.
- Guo, T., Gong, F., Lin, X., Lin, Q., Wang, X., 2018b. Experimental investigation on damage mechanism of guar gum fracturing fluid to low-permeability reservoir based on nuclear magnetic resonance. J. Energy Resour. Technol. Trans. 140, 1–11. https://doi.org/10.1115/1.4039324.
- Kang, Y.L., Luo, P.Y., 2007. Current status and prospect of key techniques for exploration and production of tight sandstone gas reservoir in China. Pet. Explor. Dev. 34 (2), 239–244. https://doi.org/10.0000/1000-0747-34-1471.
- Kang, Y., Xu, C., You, L., et al., 2014. Comprehensive evaluation of formation damage induced by working fluid loss in fractured tight gas reservoir. J. Nat. Gas Sci. Eng. 18, 353—359. https://doi.org/10.1016/j.jngse.2014.03.016.
- Lai, F.P., Li, Z.P., Zhang, T.T., Zhou, A.Q., Gong, B., 2019. Characteristics of microscopic pore structure and its influence on spontaneous imbibition of tight gas reservoir in the Ordos Basin, China. J. Pet. Sci. Eng. 172, 23–31. https://doi.org/ 10.1016/j.petrol.2018.09.020.
- Li, X., Zhang, Q., Liu, P., Li, T., Liu, G., Liu, Z., Zhang, H., 2022. Investigation on the microscopic damage mechanism of fracturing fluids to low-permeability sandstone oil reservoir by nuclear magnetic resonance. J. Petrol. Sci. Eng. 209, 109821. https://doi.org/10.1016/j.petrol.2021.109821.
- Li, Y., Guo, J., Wang, S., 2019. The damage mechanisms of fracturing fluid on production in tight gas reservoirs. Energy Proc. 158, 5988–5993. https://doi.org/10.1016/j.egypro.2019.01.521.
- Liang, T., Longoria, R.A., Lu, J., Nguyen, Q.P., DiCarlo, D.A., 2017. Enhancing hydrocarbon permeability after hydraulic fracturing: laboratory evaluations of shutins and surfactant additives. SPE J. 22 (4), 1011–1023. https://doi.org/10.2118/ 175101-PA.
- Pennycook, S., Boatner, L., 1988. Chemically Sensitive structure-imaging with a scanning transmission electron microscope. Nature 336, 565–567. https:// doi.org/10.1038/336565a0.
- Song, Z., Hou, J., Zhang, L., Chen, Z., Li, M., 2018. Experimental study on disproportionate permeability reduction caused by non-recovered fracturing fluids in tight oil reservoirs. Fuel 226, 627–634. https://doi.org/10.1016/j.fuel.2018.04.044.
- Sun, L., Zou, C., Jia, A., Wei, Y., Zhu, R., Wu, S., Guo, Z., 2019. Development characteristics and orientation of tight oil and gas in China. Pet. Explor. Dev. 46 (6),

- 1015-1026. https://doi.org/10.1016/S1876-3804(19)60264-8.
- Tan, Q, Kang, Y., You, L., Peng, H., Zhao, F., Bai, J., 2023. The role of salt dissolution on the evolution of petrophysical properties in saline-lacustrine carbonate reservoirs: pore structure, porosity—permeability, and mechanics. J. Hydrol. 618, 129257. https://doi.org/10.1016/j.jhydrol.2023.129257.
- Tian, J., Chen, Q., Qin, C., Kang, Y., Jia, Na, Xi, Z., 2022. Pore-scale systematic study on the disconnection of bulk gas phase during water imbibition using visualized micromodels. Phys. Fluids 34, 062015. https://doi.org/10.1063/5.0094930.
- Tian, J., You, L., Kang, Y., Jia, Na, 2020. Experimental investigation on water removal and gas flow during drainage process in tight rocks. J. Nat. Gas Sci. Eng. 81, 103402. https://doi.org/10.1016/j.jngse.2020.103402.
 Wang, Y., Kang, Y., Wang, D., You, L., Chen, M., Yan, X., 2022. Liquid phase blockage
- Wang, Y., Kang, Y., Wang, D., You, L., Chen, M., Yan, X., 2022. Liquid phase blockage in micro-nano capillary pores of tight condensate reservoirs. Capillarity 5 (1), 12–22. https://doi.org/10.46690/capi.2022.01.02.
- Wang, Y., Kang, Y., You, L., Xu, C., Yan, X., Lin, C., 2021. Multiscale formation damage mechanisms and control technology for deep tight clastic gas reservoirs. SPE J. 26 (6), 3877–3892. https://doi.org/10.2118/205492-PA.Wu, K., Chen, Z., Li, J., Li, X., Xu, J., Dong, X., 2017. Wettability effect on nanoconfined
- Wu, K., Chen, Z., Li, J., Li, X., Xu, J., Dong, X., 2017. Wettability effect on nanoconfined water flow. Proc. Nat. Acad. Sci 114 (13), 3358–3363. https://doi.org/10.1073/ pnas.1612608114.
- Xin, Y., Zhang, Y., Xue, P., Wang, K., Adu, E., Tontiwachwuthikul, P., 2021. The optimization and thermodynamic and economic estimation analysis for CO₂ compression-liquefaction process of CCUS system using LNG cold energy. Energy 236, 121376. https://doi.org/10.1016/j.energy.2021.121376.
- ergy 236, 121376. https://doi.org/10.1016/j.energy.2021.121376.

 Xu, G., Jiang, Y., Shi, Y., Han, Y., Wang, M., Zeng, X., 2020. Experimental investigations of fracturing fluid flowback and retention under forced imbibition in fossil hydrogen energy development of tight oil based on nuclear magnetic resonance. Int. J. Hydrogen Energy 45 (24), 13256–13271. https://doi.org/10.1016/j.ijhydene.2020.03.054.
- Xu, Z., Li, Z., Wang, C., Adenutsi, C.D., 2016. Experimental study on microscopic formation damage of low permeability reservoir caused by HPG fracturing fluid.
 J. Nat. Gas Sci. Eng. 36, 486–495. https://doi.org/10.1016/j.jngse.2016.10.063.
 Yang, Y., Xiao, W., Zhang, L., Lei, Q., Qin, C., 2023. Pore throat structure heterogeneity
- Yang, Y., Xiao, W., Zhang, L., Lei, Q., Qin, C., 2023. Pore throat structure heterogeneity and its effect on gas-phase seepage capacity in tight sandstone reservoirs: a case study from the Triassic Yanchang Formation, Ordos Basin. Petrol. Sci. 1995—8226. https://doi.org/10.1016/j.petsci.2023.03.020.
- Yao, Y., Liu, D., Cai, Y., Li, J., 2010. Advanced characterization of pores and fractures in coals by NMR and X-ray computed tomography. Sci. China Earth Sci. 53, 854–862. https://doi.org/10.1007/s11430-010-0057-4 (in Chinese).
- You, L., Zhou, Y., Kang, Y., Yang, B., Cui, Z., Cheng, Q., 2019. Fracturing fluid retention in shale gas reservoirs: mechanisms and functions. Arab. J. Geosci 12, 1–17. https://doi.org/10.1007/s12517-019-4955-2.
- Zhang, D.J., Kang, Y.L., Selvadurai, A.P., 2019. The role of phase trapping on permeability reduction in an ultra-deep tight sandstone gas reservoirs. J. Pet. Sci. Eng. 178, 311–323. https://doi.org/10.1016/j.petrol.2019.03.045.
- Zhang, D., Pang, X., Jiang, F., 2020. Characteristics and controlling factors of tight sandstone gas reservoirs in the Upper Paleozoic strata of Linxing area in the Ordos basin, China. J. Nat. Gas Sci. Eng. 75, 103135. https://doi.org/10.1016/j.jngse.2019.103135.
- Zhang, P., Lu, S., Li, J., Chen, C., Xue, H., Zhang, J., 2018. Petrophysical characterization of oil-bearing shales by low-field nuclear magnetic resonance (NMR). Mar. Petrol. Geol. 89, 775–785. https://doi.org/10.1016/j.marpetgeo.2017.11.015.
- Zhang, Y., Mao, J., Xu, T., Zhang, Z., Yang, B., Mao, J., 2019. Preparation of a novel fracturing fluid with good heat and shear resistance. RSC Adv. 9 (3), 1199e207. https://doi.org/10.1039/C8RA09483G.